Combined multi-modal assessment of glaucomatous damage with electroretinography and optical coherence tomography/angiography

Al-Nosairy, Khaldoon O.; Prabhakaran, Gokulraj T.; Pappelis, Konstantinos; Thieme, Hagen; Hoffmann, Michael B.

[Link to publication in University of Groningen/UMCG research database](#)

Article

Combined Multi-Modal Assessment of Glaucomatous Damage With Electroretinography and Optical Coherence Tomography/Angiography

Khaldoon O. Al-Nosairy[1], Gokulraj T. Prabhakaran[1], Konstantinos Pappelis[2], Hagen Thieme[1], and Michael B. Hoffmann[1,3]

[1] Department of Ophthalmology, Otto-von-Guericke University, Magdeburg, Germany
[2] Department of Ophthalmology, University of Groningen, University Medical Center, Groningen, The Netherlands
[3] Center for Behavioral Brain Sciences, Magdeburg, Germany

Purpose: To compare the diagnostic performance and to evaluate the interrelationship of electroretinographical and structural and vascular measures in glaucoma.

Methods: For 14 eyes of 14 healthy controls and 15 eyes of 12 patients with glaucoma ranging from preperimetric to advanced stages optical coherence tomography (OCT), OCT-angiography (OCT-A), and electrophysiological measures (multifocal photopic negative response ratio [mfPhNR] and steady-state pattern electroretinography [ssPERG]) were applied to assess changes in retinal structure, microvasculature, and function, respectively. The diagnostic performance was assessed via area-under-curve (AUC) measures obtained from receiver operating characteristics analyses. The interrelation of the different measures was assessed with correlation analyses.

Results: The mfPhNR, ssPERG amplitude, parafoveal (pfVD) and peripapillary vessel density (pVD), macular ganglion cell inner plexiform layer thickness (mGCIPL) and peripapillary retinal nerve fiber layer thickness (pRNFL) were significantly reduced in glaucoma. The AUC for mfPhNR was highest among diagnostic modalities (AUC: 0.88, 95% confidence interval: 0.75–1.0, $P < 0.001$), albeit not statistically different from that for macular (mGCIPL: 0.76, 0.58–0.94, $P < 0.05$; pfVD: 0.81, 0.65–0.97, $P < 0.01$) or peripapillary imaging (pRNFL: 0.85, 0.70–1.0, $P < 0.01$; pVD: 0.82, 0.68–0.97, $P < 0.01$). Combined functional/vascular measures yielded the highest AUC (mfPhNR-pfVD: 0.94, 0.85–1.0, $P < 0.001$). The functional/structural measure correlation (mfPhNR-mGCIPL correlation coefficient [r_s]: 0.58, $P = 0.001$; mfPhNR-pRNFL r_s: 0.66, $P < 0.001$) was stronger than the functional-vascular correlation (mfPhNR-pfVD r_s: 0.29, $P = 0.13$; mfPhNR-pVD r_s: 0.54, $P = 0.003$).

Conclusions: The combination of ERG measures and OCT-A improved diagnostic performance and enhanced understanding of pathophysiology in glaucoma.

Translational Relevance: Multimodal assessment of glaucoma damage improves diagnostics and monitoring of disease progression.

Introduction

Glaucoma is a progressive optic neuropathy characterized by the loss of retinal ganglion cells (RGCs) and eventually visual field (VF) defects.[1] Damage to RGCs is attributed to an increase in intraocular pressure (IOP) (mechanical theory) or primary vascular dysfunction (vascular theory).[2–5] Elevated IOP is an important risk factor for the development of primary open angle glaucoma (POAG),[6] the most prevalent glaucoma type,[7] although vascular dysfunction might be particularly critical for normal tension glaucoma (NTG).[2] However, vascular changes were also proposed for POAG.[8–10] Surrogate measures in clinical practice to estimate glaucomatous damage are

1

macular ganglion cell inner plexiform layer (mGCIPL) and peripapillary retinal nerve fiber layer (pRNFL) thickness measures obtained via optical coherence tomography (OCT)[11–13]; however, conventional structural OCT assessment does not enable the quantification of vascular changes in glaucoma.[14] Using the OCT platform for three-dimensional angiography allows for optical coherence tomography angiography (OCT-A), a recent innovation in imaging technology. In fact, OCT-A has opened the possibility of noninvasive evaluations of retina and optic nerve vasculature in glaucoma[15–19] to further our understanding of the underlying pathophysiology and to improve glaucoma detection. Vessel density parameters of macular and peripapillary areas measured with OCT-A have a similar diagnostic performance as retinal thickness measures obtained with conventional OCT (A review[20]). In fact, vessel density measures of OCT-A were strongly correlated with both structural OCT measures and functional indexes (standard automated perimetry).[20]

Although it is well known that OCT-A correlates with visual field measures,[21–23] there is limited information of OCT-A measures correlation with direct measures of retinal ganglion cell function. This gap can be filled by combining OCT-A parameters with electroretinographic (ERG) measures. Two ERG-based approaches provide sensitive information about the pathophysiology of glaucoma damage,[24] i.e. pattern ERG (PERG) and photopic negative responses (PhNR). They are therefore of paramount importance for the objective assessment of retinal function in glaucoma. The PERG is an established method with promising outcomes for glaucoma diagnosis.[25,26] The PhNR is a more recent development to quantify glaucomatous damage,[26–28] which has been applied in a conventional manner and in combination with the multifocal stimulation technique[29], that is, multifocal photopic negative response ratio (mfPhNR).[30–32]

Taken together, a combined approach of structural, vascular and functional assessment of glaucomatous retinal damage employing OCT, OCT-A and PERG/mfPhNR is of great promise to uncover the interrelationship between the different components of ocular damage in glaucoma and to shed light on the underlying patho-mechanisms. A recent study[33] demonstrated that in NTG the PhNR amplitude was correlated with macular vessel density and concluded that vascular changes might precede structural measures in early NTG. We aimed to assess such relationships for POAG. For this purpose, we correlated two types of ERG methods (PERG and mfPhNR) vs structural (OCT based) and vascular (OCT-A based) changes of macular and peripapillary

areas. This multimodal approach opens a window to assess how these structural, vascular and functional measures of retinal damage are linked to peripapillary and macular damage sites, and to each other. The aim of the present study was twofold: (i) to compare the diagnostic performance of individual measures and of combined measures of ERG and structural or vascular parameters and (ii) to elucidate the interrelation of ERG measures of retinal ganglion cell function with structural and vascular parameters and their association with macular and peripapillary sites.

Methods

Participants

Twelve glaucoma patients and 14 age-matched healthy controls were included in this observational study after giving written consent to participate in the study. The procedures followed the tenets of the declaration of Helsinki, and the protocol was approved of by the ethical committee of the Otto-von-Guericke University of Magdeburg, Germany. The study was performed in the ophthalmological department of the Otto-von-Guericke University Hospital, Magdeburg. ERG data of the study participants were acquired as part of another study.[34] In two sessions, all participants underwent best corrected visual acuity testing (BCVA) for far and near, visual field testing, OCT/-A measurements, and an ophthalmic examination.

Healthy Controls

Fourteen eyes of 14 subjects (mean age $\pm$ standard deviation [SD]: 50.2 years, 14.3) with BCVA ≥ 1 were included in the study.

Glaucoma-Group

Fifteen eyes of 12 patients (mean age $\pm$ SD: 56.8 years, 14.5; no age difference to control group [$P = 0.26$; t-test]), with open angle glaucoma were enrolled in this study. The group comprised seven preperimetric and eight perimetric glaucomatous eyes. The seven preperimetric glaucoma patients with an open anterior chamber had a glaucomatous optic disc damage defined via a vertical cup-to-disc ratio ≥ 0.7, a retinal fiber layer defect, or a local notching of the rim. The eight perimetric glaucoma eyes had glaucomatous visual field defects manifested as a cluster of three or more non-edge points all depressed on the pattern deviation plot $<5\%$ and one of which depressed $<1\%$ or abnormal corrected pattern standard deviation $<5\%$ on the Humphrey Swedish interactive threshold algorithm 24-2 (SITA fast).[35] According to the

selection criteria for the glaucoma patients' eyes (see above), incidentally only their left eyes (with three exceptions where both eyes had different stages of glaucoma damage) were included and, consequently, compared to the left eyes of the controls. An additional analysis including only the left eyes of the 12 glaucoma patients, to assess confounds of interocular correlations, yielded highly comparable results (Supplementary Tables S2 and S3).

Exclusion criteria were any systemic diseases, ocular diseases or surgeries that might affect electrophysiological recordings except cataract surgery and, in the glaucoma group, glaucoma surgery or BCVA < 0.8[36] and refractive error exceeding ±5 D or astigmatism >2 D. Insufficient quality of OCT images was also an exclusion criteria. An overview of participants' characteristics is given in Supplementary Table S1.

Visual Field Testing

Visual field sensitivities were assessed using the Swedish Interactive Threshold Algorithm 24-2 protocol (SITA-Fast) of the Humphrey Field Analyzer 3 (Carl Zeiss Meditec AG, Jena, Germany). In one control subject, visual field was tested with Octopus perimeter (dG2; dynamic strategy; Goldmann size III; OCTOPUS Perimeter 101, Haag-Streit International, Bern, Switzerland).

OCT Angiography Acquisition and Image Analysis

OCT images were acquired using the Spectralis HRA+OCT (Heidelberg Engineering, Heidelberg, Germany) equipped with the Angiography, the Glaucoma, and the Flex Module. Both eyes were scanned for macula and disc scans. OCT structural measures and angiographical images were then exported for further analysis.

Structural Measures

Averaged macular retinal nerve fiber layer thickness and ganglion cell inner plexiform layer thickness were assessed inside the 3 mm (pfRNFL and pfGCIPL, respectively) and 6 mm (mRNFL and mGCIPL, respectively) rings of ETDRS scan and exported for further analysis (Figs. 1I, 1J). The averaged peripapillary retinal nerve fiber layer thickness (pRNFL) was calculated within a 3.4 mm circle around the disc. Global indexes of macula and peripapillary structure measures, that is, mGCIPL and pRNFL thickness, respectively, were compared to other parameters.

Angiographical Measures

Spectralis OCT-A enables distinctive mapping of three vascular layers of the retina, superficial vascular plexus (SVP), intermediate capillary plexus (ICP), and deep capillary plexus (DCP).[37] We focused our analysis on the SVP layer that nourishes macular GCLIPL (mGCIPL) and peripapillary superficial vascular complex (SVC) layer, which includes the peripapillary radial capillaries supplying the pRNFL.[38,39] OCT-A images were exported in the form of transverse analysis from the Heidelberg Engineering interface. High-speed scans (20°) were used, and 768 × 768 pixel images were used. SVP (Fig. 1A), ICP, and DCP of parafovea were evaluated. Each layer was analyzed separately with a MATLAB- script[40] described below. Only the SVC of the peripapillary perfusion area was evaluated with the current script (Fig. 1D).

With the MATLAB-based script[40] used for analysis, images were imported, and one region of interest (ROI) (see below) was defined after determining the center of macula and disc for macular and disc perfusion quantification by the same investigator, respectively. SVP, ICP, and DCP were calculated automatically once the ROI center was determined manually by the investigator. Binary images of macula and optic disc were generated, and each vessel pixel and tissue pixel were represented as white and black, respectively. A local Otsu threshold[41] to binarize an image was applied to flow and no-flow signals. The ROI of the macula was a circle with 3 mm diameter centered on the macula (Figs. 1 B, 1C) and the ROI around the optic disc was a ring shaped with inner and outer radii of 1.03 and 1.84 mm (Figs. 1E, 1F). The big blood vessels of the optic nerve head (ONH) images were masked out with a Frangi vesselness filter using eigenvectors of the Hessian filter response of image[42] (Figs. 1G, 1H). To assess the reproducibility of the applied script, repeated analysis of the same OCT-A images were compared between the OCT-A data of the study population. Pairwise comparisons did not identify significant differences between the 2 iterations of image processing ($P > 0.05$). Intraclass correlations between both data sets of SVP, ICP and DCP and SVC showed excellent agreement of all measures (95% confidence interval [CI] of ICC: 0.99–1.0, $P < 0.001$).

The following parameters were evaluated: (1) Fractal dimension (FD): FD is an index of the branching complexity of the capillary network and ranges from 1 to 2, with a higher FD indicating a greater vessel branching pattern. FD was calculated based on a box-counting technique where the image is subdivided into square boxes of equal sizes and the number of boxes covering a vessel segment is counted. This was repeated for different box sizes. The logarithmized box
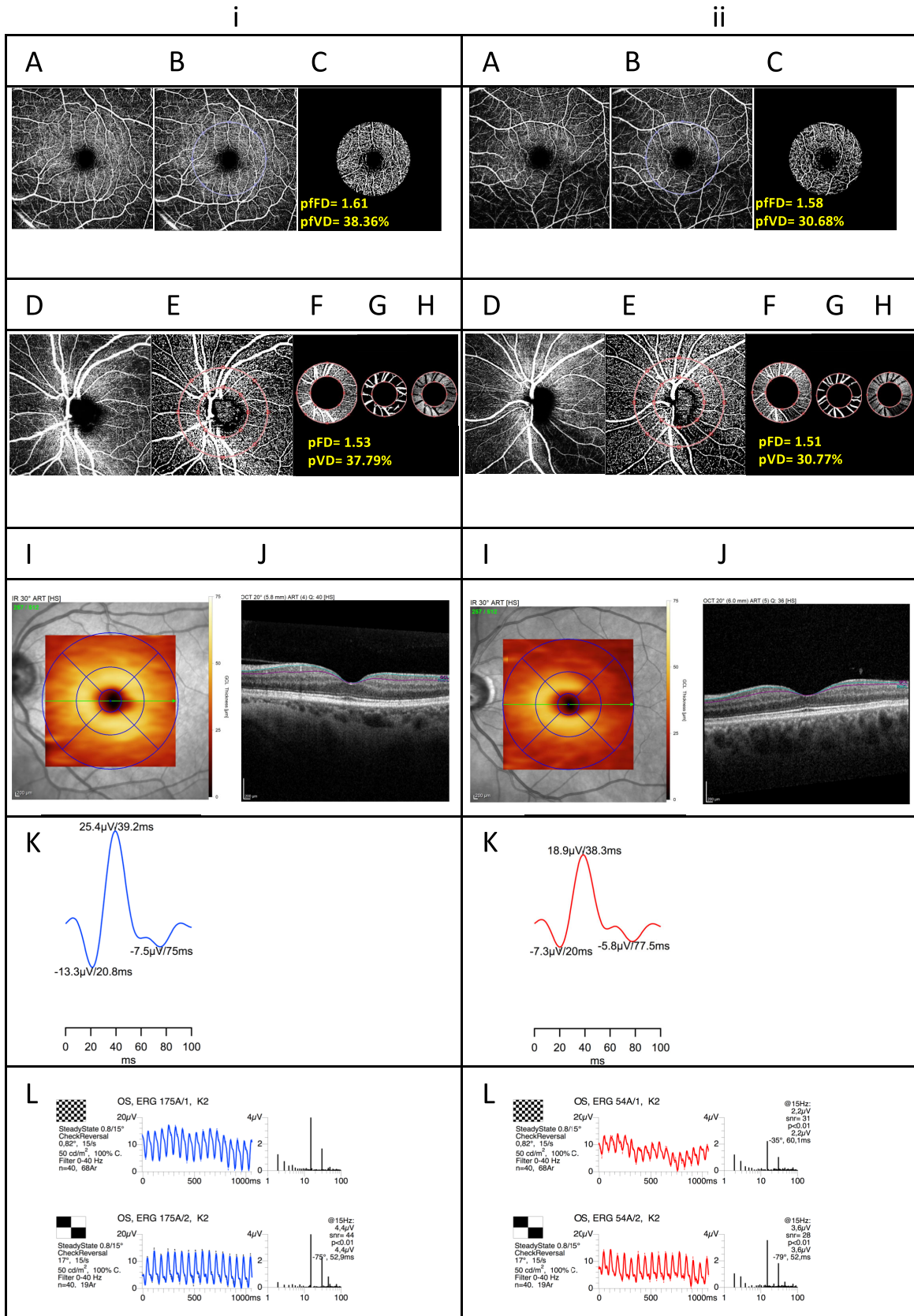
Figure 1. (**A**) OCT angiography image of the parafovea analyzing superficial vascular plexus (SVP) of (i) a representative control's and (ii) a glaucoma participant's left eye. In (**B**, **C**) offline postprocessed images (see text for details) are depicted, where (**B**) the ROI is delineated and (**C**) the ROI is used for subsequent analyses. (**D**) OCT-A of the peripapillary area extracting the superficial vascular complex. In (**E**, **F**)

→

←

offline processed images are depicted, where (**E**) is an image of the disc with delineation of ROI, (**F**) ROI of disc selected, (**G**) exclusion of big vessels from the analyzed area (**H**). In (**I**) the ETDRS scans of the macula are depicted, with a visualization of the 1, 3, 6 mm circles used for the analyses. In (**J**) a macular OCT image is shown with the ganglion cell layer embraced between the lines. (**K**) Summed mfPhNR trace with the first negativity, i.e., a wave, the first positivity, i.e., b wave, and the second negativity, i.e., the mfPhNR component. (**L**) ssPERG to 0.8 check size (*upper panel*) and 15° check size stimuli (*lower panel*) together with the frequency plot with the dominant response at the stimulation frequency, i.e., 15 Hz, and the corresponding *P* values of each response.

number was plotted vs logarithmized box size, where the FD equals the slope of the regression line.[43,44] (2) Vessel density (VD) [%]: VD is the percentage of the area occupied by capillaries. The peripapillary parameters of FD and VD were denoted as pFD and pVD to differentiate them from parafovea pfFD and pfVD parameters. In the literature, the most frequently reported measure of microvasculature in glaucoma is VD. Consequently, we focused on VD in Discussion, specifically because we obtained similar findings for FD and VD.

Visual Stimuli, Procedure, and Recordings of mfPhNR and Steady-State Pattern ERG (ssPERG)

mfPhNR

For mfPhNR recording, VERIS Science 6.4.9d13 (EDI; Electro-Diagnostic Imaging, Redwood City, CA, USA) was used for stimulus delivery and electrophysiological recordings. The stimulus comprised five visual field locations covering 48° of visual field with central and four quadrants (0°–5° and 5°–48°, respectively). A binary m-sequence of 0 (no flash) and 1 (flash) states was used for stimulation with a length of $2^9 - 1$ steps and 9 frames (frequency of stimulation: 4.2 Hz). Each step lasted 13.3 ms resulting in total recording time of 61 seconds. Two mfPhNR blocks were recorded and averaged. A monochrome CRT monitor (MDG403, Philips; P45 phosphor) was used for the stimulus presentation at 75 Hz frame rate, and the measurements were inspected in real-time on a separate monitor. In accordance with previous studies, mfPhNR were normalized to b-wave amplitude, both measured from the baseline, defined as the initial 10 ms of the epoch. The resulting mfPhNR ratio was compared between groups. We reported only the mfPhNR ratio of the summed response of five visual field locations (Fig. 1K), as a previous investigation did not reveal benefits from a spatially resolved analysis for mfPhNR-based glaucoma diagnostics.[34] The multifocal approach has the benefit to offer higher stimulation rates than conventional stimulation. Because in the present investigation we compare the ERG responses to global structural and vascular measures, we decided

beforehand to report the mfPhNR ratio of the summed response across visual field locations.

ssPERG

The EP2000 evoked potential system was used for stimulation, recording and analysis of ssPERGs[45] following the PERG-standard of the international society for clinical electrophysiology of vision.[46] The stimuli were presented at a frame rate of 75 Hz on a monochrome monitor (MDG403; Philips, Amsterdam, the Netherlands; P45 phosphor) subtending a visual angle of 62° × 49°. A 15 Hz checkerboard pattern stimulus with two check sizes (0.8° and 15°) was used for stimulation (Fig. 1L). Following established procedures,[47] the PERG ratio is calculated as an amplitude ratio of check sizes 0.8° to 15°.

In separate sessions, mfPhNR and ssPERG were recorded binocularly using active DTL (Dawson, trick Litzkow 1979, Thompson, Drasdo, 1987) electrodes (DTL Electrode ERG; Unimed Electrode Supplies, Ltd, Farnham, UK). The pupils were dilated only for the mfPhNR recordings. Further details on the procedure and recording, analysis of mfPhNR and ssPERG are given in references 26, 34, and 48.

Statistics

The mfPhNR ratio (mfPhNR) and ssPERG 0.8° amplitude (ssPERG) were calculated using IGOR (IGOR Pro; WaveMetrics, Portland, OR, USA) and exported to SPSS 26 (Statistical Package for the Social Sciences; IBM, Armonk, NY, USA), and R statistical system[49] for further analysis. The normality of the data was checked by applying the Shapiro-Walk test. Either *t*-tests or Mann-Whitney tests were conducted for cross-modal comparisons between groups, and effect sizes of these tests were also reported as a d value and U [%], which represented the probability percentage of non-overlap between two distributions.[50] Correlations between measures were calculated using Spearman's coefficient (r_s) and the 95% CI of the coefficient was calculated using a bootstrapping method. The variances explained by the correlations (r_s^2) were also calculated and reported. Receiver operating characteristics analyses were conducted

using SPSS to calculate area under curve (AUC) to discriminate between controls and glaucoma. Pairwise comparisons of all measures' AUCs were assessed to check for any significant difference between them.[51] P values were corrected for multiple testing with adjusted α-levels (P_α) using the Bonferroni-Holm correction[52] where applicable. To verify the reproducibility of the applied MATLAB analysis script, intraclass correlation of analyses between two sets of repeated analysis of the same OCT-A images and 95% CI were calculated based on absolute-agreement and two-way mixed-effects model.[53] MATLAB R2019b (MathWorks, Natick, MA, USA) was used for OCT-A image processing.

Results

Functional and Structural Parameters versus Electrophysiological and Vascular Measures

Electrophysiology

The electrophysiological measures of retinal ganglion cell function showed differential responses between the groups. The mfPhNR ratio was significantly different in glaucoma and the difference between the groups represented 75% of the nonoverlapping distribution (d = 1.7, $P_{\leq 0.025}$ = 0.0002). Similarly, the difference between healthy and glaucoma ssPERG amplitudes was statistically significant (d = 1.1, $P_{\leq 0.05}$=0.006), for effect sizes see Figures 2A and 2B.

Perimetry

On average, functional measures of glaucoma in terms of VF-MD and pattern standard deviation were statistically different between the study groups (d = 2.3, $P_{\leq 0.025}$ < 0.0001 and d = 1.3, $P_{\leq 0.05}$ = 0.004, respectively; see Table 1).

OCT

pRNFL thickness were significantly lower in glaucoma patients with a substantial effect size of 1.8 ($P_{\leq 0.025}$ = 0.001) (Figs. 2C, 2D). The mRNFL thickness was not statistically different between the groups (P > 0.05). In contrast, mGCIPL thickness was significantly lower in glaucoma (d = 1.4, $P_{\leq 0.05}$ = 0.009; see Table 1).

OCT-Angiography

In terms of vascular estimates for the parafoveal ROI, we were particularly interested in the inner retinal layer supplied by parafoveal SVP and peripapillary SVC (for effect sizes see Figs. 2E, 2H). Parafoveal FD (pfFD) (d = 1.3, $P_{\leq 0.025}$ = 0.0037) and parafoveal

VD (pfVD) (d = 1.1, $P_{\leq 0.05}$ = 0.008) were significantly reduced in glaucoma. For the peripapillary ROI perfused by SVC, pFD showed a significant decrease (d = 1.7, $P_{\leq 0.025}$ = 0.0016), as well as pVD (d = 1.5, $P_{\leq 0.05}$ = 0.0019) in glaucoma patients. It is notable that both ICP and DCP showed significant pfFD and pfVD reductions in glaucoma (P < 0.01) compared to controls (Table 1).

Discriminatory Performance of ERG, Structural Parameters, and Vascular Parameters

In terms of the discriminatory performance between controls and glaucoma, we applied receiver operating characteristics (ROC)-analyses to compare ERG measures of RGC-function (mfPhNR ratio, ssPERG amplitude), established structural (i.e., mGCLIPL thickness, pRNFL thickness) and vascular measures of parafoveal and peripapillary areas (pfFD and pfVD as well as pFD and pVD). With respect to the ERG measures of RGC-function, there was a non-significant trend for higher AUC (AUC, 95% CI, P value) for the mfPhNR ratio (0.88, 0.75–1.0, $P_{\leq 0.025}$ < 0.001) than for the ssPERG amplitude (0.81, 0.64-0.99, $P_{\leq 0.05}$ = 0.004). Therefore our further analyses were focused on the mfPhNR ratio. With respect to the structural assessment, there was a nonsignificant trend for higher AUC for pRNFL (0.85, 0.70–1.0, $P_{\leq 0.025}$ = 0.001) than for mGCIPL (0.76, 0.58–0.94, $P_{\leq 0.05}$ = 0.018). AUCs for vascular parameters were calculated for pfFD (0.82, 0.66–0.98, $P_{\leq 0.025}$ = 0.0037) and for pfVD (0.81, 0.65-0.97, $P_{\leq 0.05}$ = 0.005) compared to pFD (0.86, 0.72–0.99, $P_{<0.025}$ = 0.001) and pVD (0.82, 0.68–0.97, $P_{\leq 0.05}$ = 0.003; see Fig. 3). Finally, by conducting pairwise comparisons of ERG measures of RGC-function, structural and vascular AUCs, we found no significant differences (P > 0.05) between these measures, indicating a similar and complementary performance in terms of differentiating glaucoma from controls. By testing the combined approach to identify the highest discriminatory performance, mfPhNR-pfVD had the highest AUC for the differentiation between glaucoma and controls (AUC: 0.94; P < 0.001).

Association between ERG, Structural Parameters and Vascular Parameters

To elucidate associations between functional and other metrics, we investigated the correlation between vascular estimates of inner layers macula and peripapillary zones versus other structural and ERG
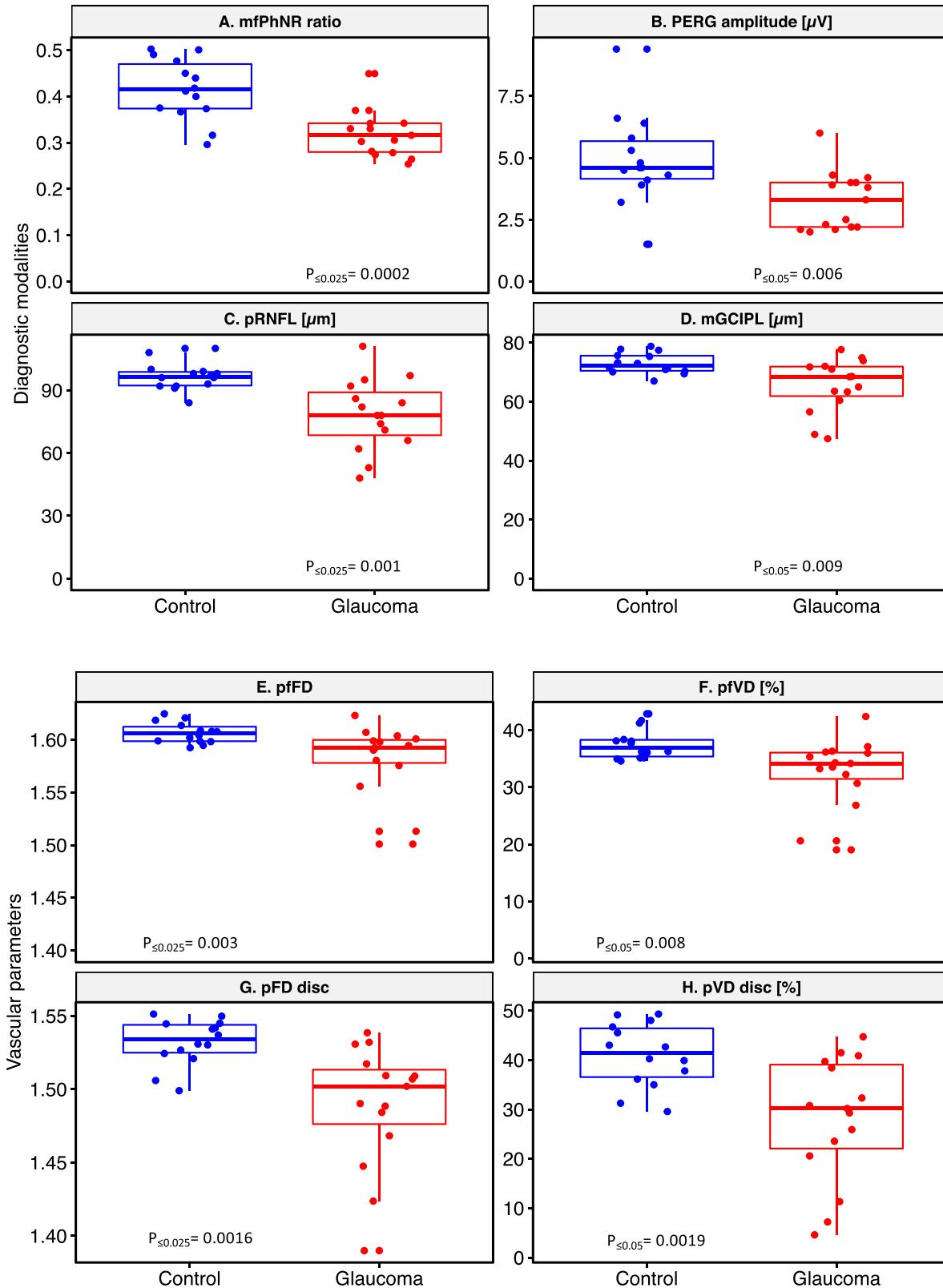
Figure 2. Cross-modal comparison of diagnostic performance. (**A**) The mfPhNR, (**B**) PERG amplitude for 0.8° check size, (**C**) averaged peripapillary retinal nerve fiber layer thickness in micrometer, and (**D**) averaged mGCIPL in micrometers. Vascular metrics of (**E**) pfFD and (**F**) pfVD. Vascular metrics of (**G**) pFD and (**H**) pVD. Independent *t*-tests were conducted except for parafoveal FD where Mann-Whitney test was performed (alpha-thresholds corrected for multiple comparisons are shown as subscripts). Panel title specifies the y-axis for each plot.

Table 1. Measures Differences Between Normal and Glaucoma Participants

Measure	Category		N	Mean	SD	t(24)	M.Diff.	d	U	P^a
Functional	MD	C	14	0.01[b]	1.48[b]	4.06[c]	2.02	2.3	85	<0.0001[c]
		G	15	−2.03[b]	4.06[b]					
	PSD	C	14	1.36[b]	0.25[b]	−2.88[c]	−0.66	1.3	65	0.004[c]
		G	15	2.02[b]	9.49[b]					
	mfPhNR	C	14	0.42	0.07	4.37	0.10	1.7	75	0.0002
		G	15	0.32	0.05					
	PERG 0.8°	C	14	4.93	1.82	2.95	1.67	1.1	59	0.006
		G	15	3.26	1.17					
	PERG ratio	C	14	1.04	0.17	2.18	0.17	0.8	47	0.038
		G	15	0.87	0.24					
Structural	pRNFL	C	14	96.71	6.66	3.86	18.25	1.8	77	0.001
		G	15	78.47	16.98					
	pfGCIPL	C	14	79.94	4.67	2.46	7.52	1.1	59	0.023
		G	15	72.43	10.80					
	mGCIPL	C	14	72.99	3.53	2.94	7.43	1.4	68	0.009
		G	15	65.56	9.07					
	pfRNFL	C	14	19.01	1.11	−0.11	−0.07	0.04	3	0.91
		G	15	19.08	1.98					
	mRNFL	C	14	25.08	1.71	1.07	1.10	0.5	33	0.30
		G	15	23.98	3.56					
Vascular	SVP pfFD	C	14	1.61[b]	0.02[b]	2.9[c]	0.03	1.3	65	0.0037[c]
		G	15	1.58[b]	0.03[b]					
	SVP pfVD	C	14	37.60	2.68	2.84	5.08	1.1	59	0.008
		G	15	32.52	6.17					
	ICP pfFD	C	14	1.58[b]	0.01[b]	3.1[c]	0.01	1.4	68	0.0016[c]
		G	15	1.57[b]	0.01[b]					
	ICP pfVD	C	14	29.48	1.93	2.84	2.97	1.1	59	0.009
		G	15	26.50	3.45					
	DCP pfFD	C	14	1.59	0.01	3.20	0.02	1.2	62	0.0034
		G	15	1.57	0.02					
	DCP pfVD	C	14	31.14	2.55	3.22	3.50	1.2	62	0.0033
		G	15	27.64	3.23					
	SVC pFD	C	14	1.53	0.02	3.70	0.04	1.7	75	0.0016
		G	15	1.49	0.04					
	SVC pVD	C	14	41.01	6.46	3.51	12.95	1.5	71	0.0019
		G	15	28.06	12.65					

P values not corrected for multiple testing due to explorative nature. C, control participants; G, glaucoma participants; d, effect size with U[%]: probability percentage of non-overlap between the two distributions; MD [dB]: mean deviation; PSD [dB], pattern standard deviation; m/pfGCIPL[μm], averaged macular/parafoveal thickness of ganglion cell layer and inner plexiform layer within 6/3 mm ETDRS scans; m/pfRNFL [μm], averaged macular/parafoveal retinal nerve fiber layer thickness within 6/3 mm ETDRS scans; PERG 0.8° [μV], steady-state pattern electroretinogram of 0.8° check size amplitude [μV]; pf/pFD, parafoveal/peripapillary fractal dimension; pf/pVD, parafoveal/peripapillary vessel density [%]; M.Diff., mean difference; n, number of eyes.

[a]T-test *P* value.
[b]Median and interquartile range.
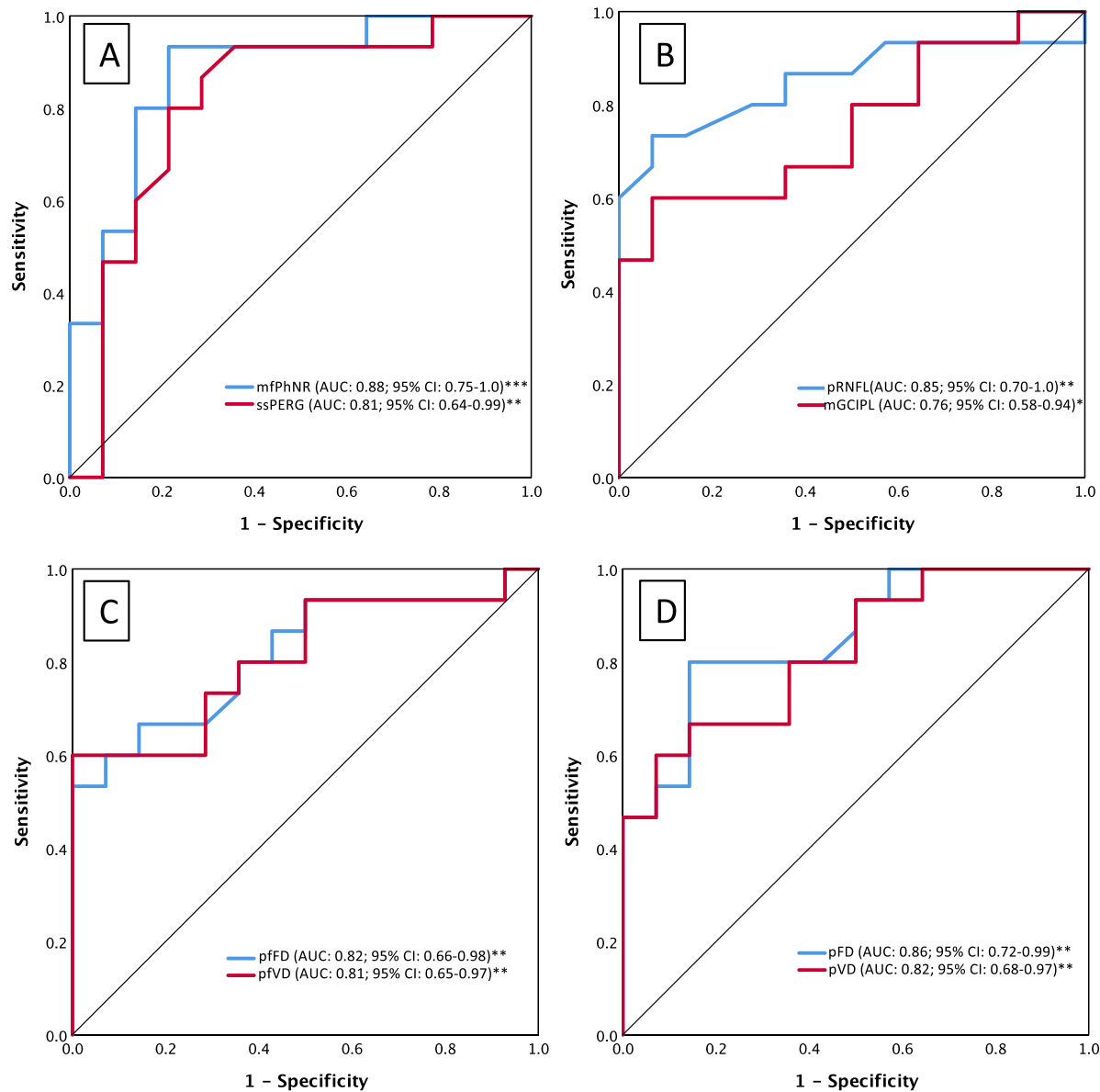[c]Mann-Whitney test z and *P* values.

Figure 3. AUC of ROC and AUC 95% CI. (**A**) Electrophysiological parameters, mfPhNR and pattern electroretinogram 0.8° amplitude (ssPERG). (**B**) Structural measures of pRNFL and mGCIPL. (**C**, **D**) vascular metrics of parafovea, which are (**C**) pfFD and pfVD versus peripapillary vascular metrics which are (**D**) pFD and pVD. *P* value significance levels are indicated where * indicates $P \leq 0.05$, ** indicates $P < 0.01$, and *** indicates $P < 0.001$ where the null hypothesis is that true area $= 0.5$.

measures of RGC-function. Both pfFD and pfVD were strongly correlated with pf/mGCLIPL thickness ($P \leq 0.001$; Table 2). Similarly vascular estimates of peripapillary perfusion showed a strong significant association with pRNFL thickness ($P \leq 0.001$). Our ERG measure of RGC-function, the mfPhNR ratio, was strongly correlated with all structural macula and peripapillary disc parameters as well as visual field-MD ($P \leq 0.001$). ssPERG amplitude was also significantly correlated to pRNFL, mGCIPL and VF-MD ($P = 0.003, 0.027,$ and 0.003, respectively), but not

to pfGCIPL ($P = 0.09$). Out of the vascular measures, the mfPhNR ratio and the ssPERG amplitude were significantly correlated only with pFD and pVD ($P < 0.01$; see Table 2 and Fig. 4). The exclusion of the two extreme data points of the correlation plots left the results essentially unchanged.

To further elucidate glaucomatous damage mechanisms, we investigated the association between ERG-based functional indexes with anatomical indexes at damage sites. ERG-based functional measures at the peripapillary site (i.e., mfPhNR-pRNFL r_s: 0.66,

Table 2. Correlations Between Functional, Structural, and Vascular Parameters

	Spearman's rho		Functional PhNR	Functional PERG	Functional MD	Structural pRNFL	Structural pfGCIPL	Structural mGCIPL	Vascular pfFD	Vascular pfVD	Vascular pFD	Vascular pVD
Functional	PERG	r	0.60^a	1								
		P	0.001									
		B^b 95% CI L	0.34									
		U	0.78									
	MD	r	0.76^a	0.53^a	1							
		P	< .001	0.003								
		B^b 95% CI L	0.53	0.19								
		U	0.89	0.80								
Structural	pRNFL	r	0.66^a	0.53	0.62^a	1						
		P	<0.001	0.003	<0.001							
		B^b 95% CI L	0.26	0.20	0.27							
		U	0.90	0.78	0.87							
	pfGCIPL	r	0.58^a	0.32	0.48^a	0.56^a	1					
		P	0.001	0.09	0.008	0.002						
		B^b 95% CI L	0.29	−0.05	0.07	0.23						
		U	0.77	0.66	0.79	0.78						
	mGCIPL	r	0.58^a	0.41^c	0.51^a	0.73^a	0.93^a	1				
		P	0.001	0.027	0.005	<0.001	<0.001					
		B^b 95% CI L	0.28	0.06	0.13	0.49	0.84					
		U	0.79	0.70	0.81	0.86	0.97					
Vascular	pfFD	r	0.34	0.24	0.52^a	0.30	0.57^a	0.57^a	1			
		P	0.07	0.20	<0.001	0.12	0.001	0.001				
		B^b 95% CI L	0.001	−0.17	0.17	−0.11	0.27	0.25				
		U	0.62	0.58	0.76	0.64	0.76	0.78				
	pfVD	r	0.29	0.21	0.52^a	0.29	0.56^a	0.57^a	0.99^a	1		
		P	0.13	0.27	0.004	0.12	0.001	0.001	<0.001			
		B^b 95% CI L	−0.05	−0.18	0.20	−0.12	0.25	0.25	0.98			
		U	0.58	0.55	0.74	0.63	0.76	0.80	1.0			
	pFD	r	0.56^a	0.52^a	0.54^a	0.80^a	0.49^a	0.65^a	0.39^c	0.37^c	1	
		P	0.002	0.004	0.002	<0.001	0.007	< 0.001	0.037	0.046		
		B^b 95% CI L	0.19	0.19	0.18	0.60	0.12	0.33	0.04	0.02		
		U	0.82	0.75	0.79	0.92	0.76	0.86	0.067	0.65		
	pVD	R	0.54^a	0.49^a	0.48^a	0.79^a	0.45^c	0.64^a	0.35	0.34	0.99^a	1
		P	0.003	0.007	0.008	<0.001	0.014	<0.001	0.07	0.07	<0.001	
		B^b 95% CI L	0.14	0.19	0.08	0.57	0.06	0.34	−0.07	−0.07	0.98	
		U	0.82	0.74	0.78	0.93	0.73	0.84	0.66	0.65	1.0	

Included eyes: 14 eyes of 14 control subjects and 15 eyes (12 left/3 right eyes) of 12 glaucoma subjects. Peripapillary measures: Blue font; macular/parafoveal measures: green fonts. Conventions as Table 1. U, upper limit of 95% CI; L, lower limit of 95% CI.

^{a}Correlation is significant at the 0.01 level (uncorrected, 2-tailed, blue background).

^{b}Bootstrap results are based on 1000 bootstrap samples.

^{c}Correlation is significant at the 0.05 level (uncorrected, 2-tailed, light blue background).

P value > 0.05 White background.

$P = 0.0001$ and mfPhNR-pVD r_s: 0.54, $P = 0.003$) exceeded those at the macular site (i.e. mfPhNR-mGCIPL r_s: 0.58, $P = 0.001$ and mfPhNR-pfVD r_s: 0.29, $P = 0.13$).

Discussion

Applying a set of complementary retinal imaging modalities we demonstrated a significant effect of glaucoma on vascular (OCT-A; parafoveal vessel density "pfVD" and fractal dimension "pfFD" and peripapillary pVD and pFD), electrophysi-ological (mfPhNR ratio and ssPERG amplitude) and structural measures (OCT; mGCIPL/pRNFL). These measures had equivalently high discrimina-tory performance, which further improved for the combination of the methods. The ERG measures of retinal ganglion cell function were more strongly associated with structural than with vascular measures.

Our findings of significant changes in the ocular microvasculature (VD) in glaucoma support previous studies, that demonstrated glaucomatous changes in the VD of the macular/parafoveal superficial layers[16,18,54–56] and the peripapillary area.[22,54–57]
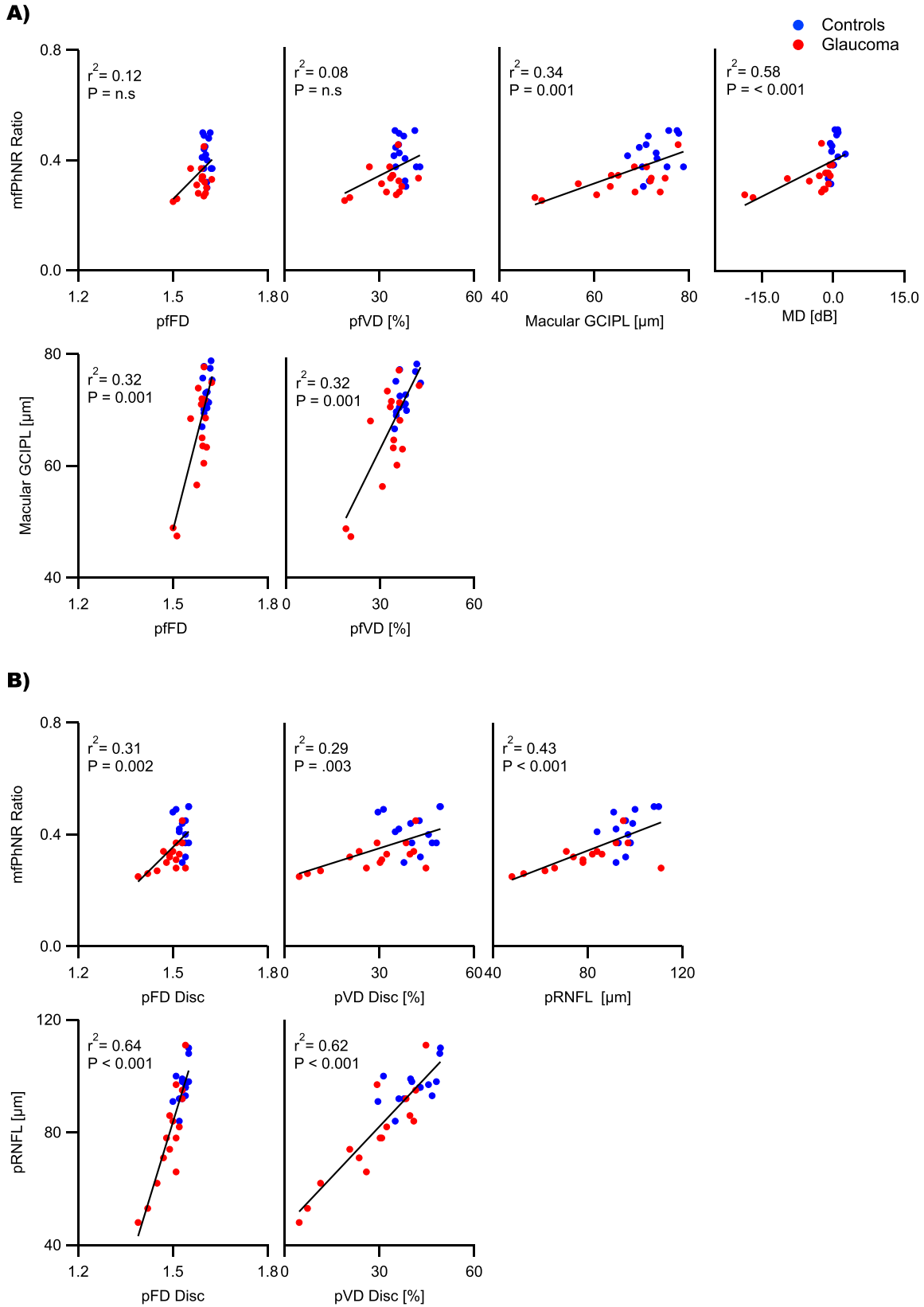
Figure 4. (**A**) Correlation plots of mfPhNR (*upper panel*) versus pfFD and pfVD mGCIPL and visual field mean deviation (dB) and of mGCIPL (*bottom*) versus pfFD and pfVD measures. (**B**) Correlation plots of mfPhNR (*top*) versus peripapillary perfusion metrics and pRNFL and of pRNFL (*bottom*) versus pFD and pVD. r_s^2 = coefficient of determination. n.s= nonsignificant association.

Furthermore, they are in agreement with investigations that demonstrated glaucoma associated changes in mfPhNR and PERG[25,26,34] and mGCIPL and pRNFL.[11–13] We considerably extended these studies by demonstrating an association between ERG-based functional and anatomical indexes, as well as an enhanced diagnostic efficacy of combined ERG-based functional indexes with vascular indexes.

Cross-Modal Comparison of Glaucoma Detection

To assess the benefit of any of the applied modalities for glaucoma detection, we conducted ROC analyses and compared their outcome measures, that is, AUC. The only previous cross-modal study addressing this for early glaucoma detection,[58] demonstrated ssPERG to have a higher performance (AUC = 0.92) than whole image VD in macula and disc (AUC= 0.80 and 0.74, respectively) and ganglion cell complex thickness (AUC = 0.74). In the current study, the highest discrimination performance was observed for the mfPhNR (not tested in[58]; AUC = 0.88), albeit not being significantly different from other measures' AUCs. Subsequently, we investigated the effect of combining ERG measures of RGC-function with structural or vascular measures. In fact, the combination of mfPhNR with pfVD AUCs yielded the highest AUC (0.94; $P < 0.001$), indicating an improvement of diagnostic performance. In addition to its relevance for glaucoma diagnosis, the improved performance for the combined assessment with pfVD might also suggest that the ERG measures of RGC-function and OCT-A measures reflect distinctive glaucomatous damage mechanisms within the retina. It should be noted, however, that, as an alternative, the enhancement might also be due to decreasing the effect of noise by pooling data from different modalities.

Association of ERG, Structural, and Vascular Measures in Glaucoma

Given the relation of vascular changes with glaucoma, it is currently still unresolved, whether these are secondary or primary events associated with RGCs damage.[2] Previous OCT-A studies are inconclusive because they found structural changes either to precede[17,59,60] or succeed[33,61] vascular changes in glaucoma. We investigated the interrelation of these measures with the sensitive measures of RGC-function, mfPhNR, and ssPERG amplitude to elucidate glaucomatous damage mechanisms. For this purpose, we compared the association of retinal ganglion cell dysfunction with specific changes (i) in fundus anatomy, that is, microvasculature (OCT-A) and retinal structure (OCT), and (ii) at damage sites, that is, macular and peripapillary sites: (i) Fundus anatomy: We reported a stronger correlation of RGC-function (mfPhNR/ssPERG) with retinal structure ($r_s \leq 0.66$) than with the microvasculature ($r_s \leq 0.56$). In contrast, for NTG the reverse pattern was recently reported,[33] that is, a stronger association of PhNR with measures of macular/parafoveal microvasculature ($r \leq 0.42$). Taken together, these findings support the current view that NTG is more strongly associated with vascular damage mechanisms than POAG. (ii) Damage sites: The measures of RGC-function were more strongly associated with peripapillary than with macular structural and vascular measures (mfPhNR with pRNFL and pVD r_s: 0.66 and 0.54, respectively; mfPhNR with mGCIPL and pfVD r_s: 0.58 and 0.29, respectively). This suggests that damage mechanisms exert their action preferentially at the peripapillary zone. It must be noted, however, that in the present study glaucomatous damage ranged from preperimetric to advanced glaucoma, such that, for example, early-stage changes of the macula[13,62,63] might not have been relevant.

Limitations

A small sample size, because of strict inclusion criteria and extensive diagnostic methods used, is a limiting factor for the findings of this study.

Practical Considerations and Potential Applications

We provide proof-of-concept for the use of ERG to further our understanding of glaucoma pathophysiology. Because we demonstrated that the combined use of ERG and vascular measures improved the detection of glaucomatous damage, it is of great promise to study their diagnostic role in borderline cases, such as glaucoma suspects, as well as for the follow-up of glaucomatous damage because ERG offers means to monitor RGC dysfunction that might precede vascular/structural damage.

In conclusion, combining ERG and OCT-A measures may improve the assessment and eventually the management of glaucoma. Follow-up studies comparing the effects of glaucoma on retinal electrophysiology, microvasculature, and structure with larger sample sizes and using longitudinal designs are of promise to further explore the pathophysiology of glaucoma.

Acknowledgments

References

1. Kwon YH, Fingert JH, Kuehn MH, Alward WLM. Primary Open-Angle Glaucoma. *N Engl J Med*. 2009;360(11):1113–1124.
2. Mansouri K. Optical coherence tomography angiography and glaucoma: searching for the missing link. *Expert Rev Med Devices*. 2016;13(10):879–880.
3. Flammer J. The vascular concept of glaucoma. *Surv Ophthalmol*. 1994;38:S3–S6.
4. Flammer J, Orgül S, Costa VP, et al. The impact of ocular blood flow in glaucoma. *Prog Retin Eye Res*. 2002;21(4):359–393.
5. Halpern DL, Grosskreutz CL. Glaucomatous optic neuropathy: mechanisms of disease. *Ophthalmol Clin N Am*. 2002;15(1):61–68.
6. Bahrami H. Causal inference in primary open angle glaucoma: specific discussion on intraocular pressure. *Ophthalmic Epidemiol*. 2006;13(4):283–289.
7. Tham Y-C, Li X, Wong TY, Quigley HA, Aung T, Cheng C-Y. Global prevalence of glaucoma and projections of glaucoma burden through 2040: a systematic review and meta-analysis. *Ophthalmology*. 2014;121(11):2081–2090.
8. Mroczkowska S, Benavente-Perez A, Negi A, Sung V, Patel SR, Gherghel D. Primary open-angle glaucoma vs normal-tension glaucoma: the vascular perspective. *JAMA Ophthalmol*. 2013;131(1):36–43.
9. Bonomi L, Marchini G, Marraffa M, Bernardi P, Morbio R, Varotto A. Vascular risk factors for primary open angle glaucoma: the Egna-Neumarkt Study. *Ophthalmology*. 2000;107(7):1287–1293.
10. Salowe R, Salinas J, Farbman NH, et al. Primary open-angle glaucoma in individuals of African descent: a review of risk factors. *J Clin Exp Ophthalmol*. 2015;6(4):450.
11. Mwanza J-C, Durbin MK, Budenz DL, et al. Glaucoma diagnostic accuracy of ganglion cell-inner plexiform layer thickness: comparison with nerve fiber layer and optic nerve head. *Ophthalmology*. 2012;119(6):1151–1158.
12. Oddone F, Lucenteforte E, Michelessi M, et al. Macular versus retinal nerve fiber layer parameters for diagnosing manifest glaucoma: a systematic review of diagnostic accuracy studies. *Ophthalmology*. 2016;123(5):939–949.
13. Kim YK, Ha A, Na KI, Kim HJ, Jeoung JW, Park KH. Temporal relation between macular ganglion cell-inner plexiform layer loss and peripapillary retinal nerve fiber layer loss in glaucoma. *Ophthalmology*. 2017;124(7):1056–1064.
14. Gao SS, Jia Y, Zhang M, et al. Optical coherence tomography angiography. *Invest Ophthalmol Vis Sci*. 2016;57(9):OCT27–OCT36.
15. Jia Y, Tan O, Tokayer J, et al. Split-spectrum amplitude-decorrelation angiography with optical coherence tomography. *Opt Express*. 2012;20(4):4710–4725.
16. Penteado RC, Zangwill LM, Daga FB, et al. Optical coherence tomography angiography macular vascular density measurements and the central 10-2 visual field in glaucoma. *J Glaucoma*. 2018;27(6):481–489.
17. Kim SB, Lee EJ, Han JC, Kee C. Comparison of peripapillary vessel density between preperimetric and perimetric glaucoma evaluated by OCT-angiography. *PloS One*. 2017;12(8):e0184297.
18. Akil H, Chopra V, Al-Sheikh M, et al. Swept-source OCT angiography imaging of the macular capillary network in glaucoma. *Br J Ophthalmol*. 2018;102(4):515–519.
19. Yarmohammadi A, Zangwill LM, Diniz-Filho A, et al. Optical coherence tomography angiography vessel density in healthy, glaucoma suspect, and glaucoma eyes. *Invest Ophthalmol Vis Sci*. 2016;57(9):OCT451–OCT459.
20. Van Melkebeke L, Barbosa-Breda J, Huygens M, Stalmans I. Optical coherence tomography angiography in glaucoma: a review. *Ophthalmic Res*. 2018;60(3):139–151.
21. Ghahari E, Bowd C, Zangwill LM, et al. Association of macular and circumpapillary microvasculature with visual field sensitivity in advanced glaucoma. *Am J Ophthalmol*. 2019;204:51–61, doi:10.1016/j.ajo.2019.03.004.
22. Liu L, Jia Y, Takusagawa HL, et al. Optical coherence tomography angiography of the peri-

papillary retina in glaucoma. *JAMA Ophthalmol.* 2015;133(9):1045–1052.

23. Yarmohammadi A, Zangwill LM, Diniz-Filho A, et al. Relationship between optical coherence tomography angiography vessel density and severity of visual field loss in glaucoma. *Ophthalmology.* 2016;123(12):2498–2508.

24. Wilsey LJ, Fortune B. Electroretinography in glaucoma diagnosis. *Curr Opin Ophthalmol.* 2016;27(2):118–124.

25. Bode SFN, Jehle T, Bach M. Pattern electroretinogram in glaucoma suspects: new findings from a longitudinal study. *Invest Ophthalmol Vis Sci.* 2011;52(7):4300–4306.

26. Preiser D, Lagrèze WA, Bach M, Poloschek CM. Photopic negative response versus pattern electroretinogram in early glaucoma. *Invest Ophthalmol Vis Sci.* 2013;54(2):1182–1191.

27. Viswanathan S, Frishman LJ, Robson JG, Walters JW. The photopic negative response of the flash electroretinogram in primary open angle glaucoma. *Invest Ophthalmol Vis Sci.* 2001;42(2):514–522.

28. Kirkiewicz M, Lubiński W, Penkala K. Photopic negative response of full-field electroretinography in patients with different stages of glaucomatous optic neuropathy. *Doc Ophthalmol.* 2016;132(1):57–65.

29. Sutter EE. Imaging visual function with the multifocal m-sequence technique. *Vis Res.* 2001;41(10-11):1241–1255.

30. Kaneko M, Machida S, Hoshi Y, Kurosaka D. Alterations of photopic negative response of multifocal electroretinogram in patients with glaucoma. *Curr Eye Res.* 2015;40(1):77–86.

31. Kato F, Miura G, Shirato S, Sato E, Yamamoto S. Correlation between N2 amplitude of multifocal ERGs and retinal sensitivity and retinal nerve fiber layer thickness in glaucomatous eyes. *Doc Ophthalmol Adv Ophthalmol.* 2015;131(3):197–206.

32. Van Alstine AW, Viswanathan S. Test-retest reliability of the multifocal photopic negative response. *Doc Ophthalmol.* 2017;134(1):25–36.

33. Honda H, Anraku A, Ishida K, Enomoto N, Tomita G. Relationship between macular vessel density and focal electroretinograms in early normal tension glaucoma. *Curr Eye Res.* 2019;44(7):753–759.

34. Al-Nosairy KO, Thieme H, Hoffmann MB. Diagnostic performance of multifocal photopic negative response, pattern electroretinogram and optical coherence tomography in glaucoma. *Experimental Eye Research.* 2020;200:108242.

35. Anderson DR, Patella VM. *Automated static perimetry.* St. Louis: Mosby; 1999.

36. Bach M, Mathieu M. Different effect of dioptric defocus vs. light scatter on the pattern electroretinogram (PERG). *Doc Ophthalmol.* 2004;108(1):99–106.

37. Hosari S, Hohberger B, Theelke L, Sari H, Lucio M, Mardin CY. OCT angiography: measurement of retinal macular microvasculature with Spectralis II OCT angiography—reliability and reproducibility. *Ophthalmol J Int Ophtalmol Int J Ophthalmol Z Augenheilkd.* 2020;243(1):75–84.

38. Iwasaki M, Inomata H. Relation between superficial capillaries and foveal structures in the human retina. *Invest Ophthalmol Vis Sci.* 1986;27(12):1698–1705.

39. Campbell JP, Zhang M, Hwang TS, et al. Detailed vascular anatomy of the human retina by projection-resolved optical coherence tomography angiography. *Sci Rep.* 2017;7:42201.

40. Pappelis K, Jansonius NM. Quantification and repeatability of vessel density and flux as assessed by optical coherence tomography angiography. *Transl Vis Sci Technol.* 2019;8(3):3.

41. Otsu N. A threshold selection method from gray-level histograms. *IEEE Trans Syst Man Cybern.* 1979;9(1):62–66.

42. Frangi AF, Niessen WJ, Vincken KL, Viergever MA. Multiscale vessel enhancement filtering. In: Wells WM, Colchester A, Delp S, eds. *Medical Image Computing and Computer-Assisted Intervention — MICCAI'98.* Lecture Notes in Computer Science. Berlin: Springer; 1998:130–137.

43. Masters BR. Fractal analysis of the vascular tree in the human retina. *Annu Rev Biomed Eng.* 2004;6(1):427–452.

44. Reif R, Qin J, An L, Zhi Z, Dziennis S, Wang R. Quantifying optical microangiography images obtained from a spectral domain optical coherence tomography system. *Int J Biomed Imaging.* 2012;2012:509783.

45. Bach M. Bach-Freiburg evoked potentials. Available at: http://localhost:4000/ep2000/. Accessed January 14, 2019.

46. Bach M, Brigell MG, Hawlina M, et al. ISCEV standard for clinical pattern electroretinography (PERG): 2012 update. *Doc Ophthalmol.* 2013;126(1):1–7.

47. Bach M, Hoffmann MB. Update on the pattern electroretinogram in glaucoma. *Optom Vis Sci.* 2008;85(6):386.

48. Al-Nosairy KO, van den Bosch JJON, Pennisi V, et al. Use of a novel telemetric sensor to study interactions of intraocular pressure and ganglion-cell

function in glaucoma [published online ahead of print July 29, 2020]. *Br J Ophthalmol*, doi:10.1136/bjophthalmol-2020-316136.

49. R Core Team. *R: The R Project for Statistical Computing. R: A language and environment for statistical computing*. Vienna, Austria: R Foundation for Statistical Computing; 2013.

50. Fritz CO, Morris PE, Richler JJ. Effect size estimates: current use, calculations, and interpretation. *J Exp Psychol Gen*. 2012;141(1):2–18.

51. Hanley JA, McNeil BJ. A method of comparing the areas under receiver operating characteristic curves derived from the same cases. *Radiology*. 1983;148(3):839–843.

52. Holm S. A simple sequentially rejective multiple test procedure. *Scand J Stat*. 1979;6(2):65–70.

53. Koo TK, Li MY. A guideline of selecting and reporting intraclass correlation coefficients for reliability research. *J Chiropr Med*. 2016;15(2):155–163.

54. Rao HL, Pradhan ZS, Weinreb RN, et al. Regional comparisons of optical coherence tomography angiography vessel density in primary open-angle glaucoma. *Am J Ophthalmol*. 2016;171:75–83.

55. Yarmohammadi A, Zangwill LM, Manalastas PIC, et al. Peripapillary and macular vessel density in patients with primary open-angle glaucoma and unilateral visual field loss. *Ophthalmology*. 2018;125(4):578–587.

56. Chung JK, Hwang YH, Wi JM, Kim M, Jung JJ. Glaucoma diagnostic ability of the optical coherence tomography angiography vessel density parameters. *Curr Eye Res*. 2017;42(11):1458–1467.

57. Scripsema NK, Garcia PM, Bavier RD, et al. Optical coherence tomography angiography analysis of perfused peripapillary capillaries in primary open-angle glaucoma and normal-tension glaucoma. *Invest Ophthalmol Vis Sci*. 2016;57(9):OCT611–OCT620.

58. Kurysheva NI, Maslova EV, Zolnikova IV, Fomin AV, Lagutin MB. A comparative study of structural, functional and circulatory parameters in glaucoma diagnostics. *PloS One*. 2018;13(8):e0201599.

59. Lee EJ, Kim S, Hwang S, Han JC, Kee C. Microvascular compromise develops following nerve fiber layer damage in normal-tension glaucoma without choroidal vasculature involvement. *J Glaucoma*. 2017;26(3):216–222.

60. Akagi T, Iida Y, Nakanishi H, et al. Microvascular density in glaucomatous eyes with hemifield visual field defects: an optical coherence tomography angiography study. *Am J Ophthalmol*. 2016;168:237–249.

61. Shoji T, Zangwill LM, Akagi T, et al. Progressive macula vessel density loss in primary open angle glaucoma: a longitudinal study. *Am J Ophthalmol*. 2017;182:107–117.

62. Hood DC, Raza AS, de Moraes CGV, Liebmann JM, Ritch R. Glaucomatous damage of the macula. *Prog Retin Eye Res*. 2013;32:1–21.

63. Kim YK, Jeoung JW, Park KH. Inferior macular damage in glaucoma: its relationship to retinal nerve fiber layer defect in macular vulnerability zone. *J Glaucoma*. 2017;26(2):126–132.